ARTICLE

doi:10.1038/nature10109

Crystal structure of the FimD usher bound to its cognate FimC–FimH substrate

Gilles Phan[1]*, Han Remaut[1,2]*, Tao Wang[3]*, William J. Allen[1]*, Katharina F. Pirker[1], Andrey Lebedev[4], Nadine S. Henderson[5], Sebastian Geibel[1], Ender Volkan[6], Jun Yan[1], Micha B. A. Kunze[1], Jerome S. Pinkner[6], Bradley Ford[6,7], Christopher W. M. Kay[1,8,9], Huilin Li[3,10], Scott J. Hultgren[6], David G. Thanassi[5] & Gabriel Waksman[1,9]

Type 1 pili are the archetypal representative of a widespread class of adhesive multisubunit fibres in Gram-negative bacteria. During pilus assembly, subunits dock as chaperone-bound complexes to an usher, which catalyses their polymerization and mediates pilus translocation across the outer membrane. Here we report the crystal structure of the full-length FimD usher bound to the FimC–FimH chaperone–adhesin complex and that of the unbound form of the FimD translocation domain. The FimD–FimC–FimH structure shows FimH inserted inside the FimD 24-stranded β-barrel translocation channel. FimC–FimH is held in place through interactions with the two carboxy-terminal periplasmic domains of FimD, a binding mode confirmed in solution by electron paramagnetic resonance spectroscopy. To accommodate FimH, the usher plug domain is displaced from the barrel lumen to the periplasm, concomitant with a marked conformational change in the β-barrel. The amino-terminal domain of FimD is observed in an ideal position to catalyse incorporation of a newly recruited chaperone–subunit complex. The FimD–FimC–FimH structure provides unique insights into the pilus subunit incorporation cycle, and captures the first view of a protein transporter in the act of secreting its cognate substrate.

Gram-negative pathogens commonly interact with their environment using long, linear, surface-exposed protein appendages called pili. In uropathogenic *Escherichia coli*, type 1 pili carry at their distal end a dedicated mannose-specific adhesin, FimH, that is responsible for the attachment of bacteria to the bladder epithelium and their subsequent internalization and biofilm-like organization inside the urothelial cells.

Type 1 pili are representative of a large class of non-covalently linked fibres on the surface of gram-negative bacteria, synthesized via the conserved chaperone/usher pathway[1–3]. Type 1 pili are composed of four different subunit types (FimH, FimG, FimF and FimA). The adhesin FimH and two linker subunits FimG and FimF form a short flexible fibrillar tip that is attached to an extended rigid and helically wound rod of thousands of FimA subunits (Supplementary Fig. 1a)[4–6]. Subunits cross the inner membrane via the SecYEG secretory pathway. In the periplasm, folding and stability of the subunits require formation of a binary complex with the FimC chaperone[7,8]. Chaperone–subunit complexes are then targeted to the outer membrane usher, FimD, which catalyses the ordered polymerization of subunits and enables the translocation of the growing fibre across the outer membrane in a self-energized process[9,10].

All pilus subunits (or pilins) exhibit an incomplete Ig-like fold, characterized by the absence of the C-terminal β-strand[11–13] (Supplementary Fig. 1b), leaving a deep hydrophobic groove on the subunit surface (Supplementary Fig. 1c). As a result, pilus subunits are unstable on their own, unless in a chaperone–subunit complex or bound to an adjacent subunit within the pilus. Both chaperone–subunit and subunit–subunit interactions involve a fold-complementation mechanism whereby the subunit's non-canonical Ig-fold is complemented *in trans* by, respectively, an extended β-strand in the N-terminal domain of the chaperone (strand G1) or a 10 to 20-residue-long peptide extension at the N terminus of the adjacent subunit (called the N-terminal extension or Nte)[11–14] (Supplementary Fig. 1b). During subunit polymerization, the chaperone donor strand binding the subunit's hydrophobic groove (an interaction termed donor-strand complementation or DSC) is replaced by the Nte of the newly incorporated subunit in a process called donor-strand exchange (DSE)[11] (Supplementary Fig. 1b).

The structure of the translocation domain of the P pilus usher PapC in its inactive state revealed a 24-stranded β-barrel protein[15]. The loop between strands 6 and 7 of the β-barrel holds an 80-residue insertion that forms a plug domain that, in the non-engaged usher, resides in the barrel lumen, gating the usher channel shut. In addition to the translocation domain, ushers (~800 residues) contain a ~120-residue N-terminal domain (NTD) responsible for chaperone–subunit binding and recruitment[16–18] and a ~170 residue C-terminal domain (CTD) of poorly understood function[19,20] (Fig. 1a). How these domains cooperate to recruit chaperone–subunit complexes, catalyse subunit polymerization, and translocate the nascent pilus through the membrane is unknown. To provide insights into these processes, we present here the crystal structure of the FimD usher bound to its cognate FimC–FimH chaperone–adhesin substrate and that of the non-engaged FimD usher translocation domain.

Structure of the FimD–FimC–FimH complex

A stoichiometric complex containing the type 1 pilus usher FimD bound to the FimC–FimH chaperone–adhesin complex (Fig. 1a)

[1]Institute of Structural and Molecular Biology, University College London and Birkbeck College, Malet Street, London WC1E 7HX, UK. [2]Structural & Molecular Microbiology and Structural Biology Brussels, VIB - Vrije Universiteit Brussels, 1050 Brussels, Belgium. [3]Biology Department, Brookhaven National Laboratory, Upton, New York 11973, USA. [4]Department of Chemistry, University of York, York YO10 5YW, UK. [5]Center for Infectious Diseases and Department of Molecular Genetics & Microbiology, Stony Brook University, Stony Brook, New York 11794, USA. [6]Department of Molecular Microbiology and Center for Women's Infectious Disease Research, Washington University School of Medicine, Saint Louis, Missouri 63110, USA. [7]Department of Pathology and Immunology, Washington University, St Louis, Missouri 63110, USA. [8]London Centre for Nanotechnology, University College London, 17–19 Gordon Street, London WC1H 0AH, UK. [9]Research Department of Structural and Molecular Biology, University College London, Gower Street, London WC1E 6BT, UK. [10]Department of Biochemistry and Cell Biology, Stony Brook University, Stony Brook, New York 11794, USA.
*These authors contributed equally to this work.

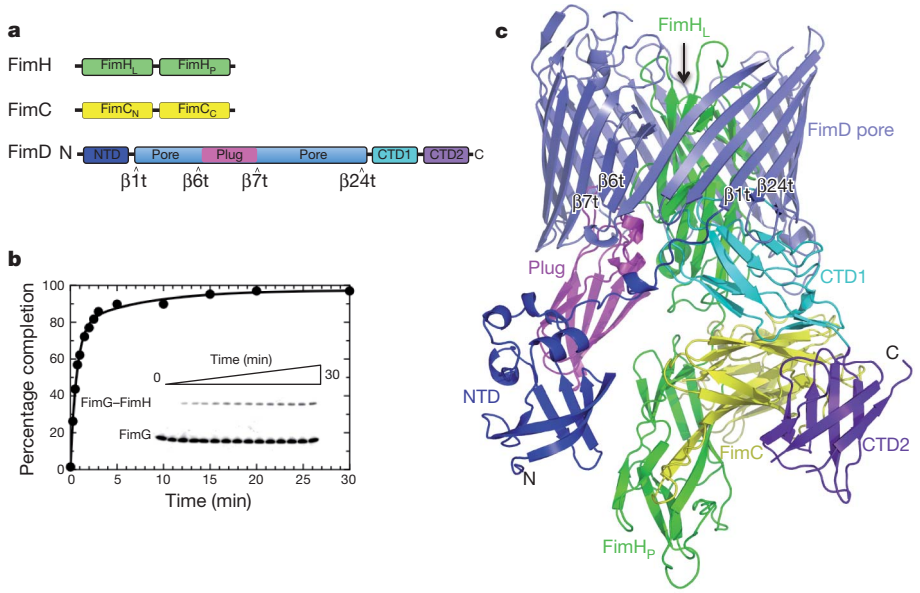

Figure 1 | Structure of the FimD–FimC–FimH complex. **a**, Schematic diagram of domain organization of FimH (FimH$_L$, lectin domain; FimH$_P$, pilin domain), FimC (FimC$_N$, N-terminal domain; FimC$_C$, C-terminal domain) and FimD (see text). **b**, Activity assay demonstrating that the purified FimD–FimC–FimH complex is functional. FimD–FimC–FimH was challenged at $t = 0$ by the FimC–FimG$^{S92C[A647]}$ complex fluorescently labelled by Alexa 647 reacted on residue 92 of FimG (see position of residue 92 in Supplementary Fig. 2b). Intensity of the fluorescent FimG–FimH band (the DSE product) was used to assess the percentage progress of the DSE reaction. Inset, raw SDS–PAGE gel visualized as described in Methods. Each band represents a time point. **c**, Side view ribbon representation of the FimD–FimC–FimH structure, with FimH in green, FimC in yellow and the FimD NTD, β-barrel, plug, CTD1 and CTD2 in blue, slate, magenta, cyan and purple, respectively. β1t, β6t and β7t, and β24t indicate the β-barrel strands (see secondary structure labelling nomenclature in Supplementary Fig. 3a) connecting the barrel to the NTD, the plug and the CTDs, respectively.

was purified and shown to be active (Fig. 1b). It was then crystallized and its structure determined to 2.8 Å resolution (Fig. 1c, Supplementary Fig. 2a, Supplementary Table 1 and Methods). Like PapC, FimD contains a 24-stranded β-barrel (residues 139–665), interrupted by a plug domain (residues 241–324) inserted in the periplasmic loop linking strands 6 and 7 (Figs 1, 2, and topology diagram in Supplementary Fig. 3). However, in contrast to the PapC structure, which captured the non-activated, unbound translocation channel, the plug domain in the FimD–FimC–FimH complex now resides in the periplasm, underneath the translocation domain and next to the NTD (Fig. 1c and Supplementary Fig. 4). The usher NTD has been shown to form a binding site for chaperone–subunit complexes, including FimC–FimH[16–18]. In the FimD–FimC–FimH structure, however, the NTD lies idle, making no interactions with FimC (see below); the FimC–FimH complex instead is bound to two Ig-like domains formed at the usher C terminus, CTD1 and CTD2 (residues 666–750 and 751–834, respectively).

FimH is a two-domain protein (Fig. 1a), where the N-terminal lectin domain (residues 1–157; FimH$_L$) is responsible for receptor binding, and the C-terminal or pilin domain (residues 158–279; FimH$_P$) forms the interacting region with either the chaperone within the chaperone–adhesin complex in the periplasm or with the adjacent subunit (FimG) within the pilus[12]. In the ternary FimD–FimC–FimH complex, FimC stabilizes the FimH pilin domain via a typical DSC fold-complementation interaction, which remains unchanged compared to the FimC–FimH complex alone[12]. Remarkably, the FimH lectin domain inserts into the lumen of the translocation channel, traversing the entire length of the channel, its tip exposed on the extracellular side of the usher. FimD is the first transporter to be visualized with a substrate protein inserted through its lumen. The FimH pilin domain and the FimC chaperone are located underneath the pore.

Usher activation involves a large conformational change in the β-barrel domain

The FimC–FimH complex is the first chaperone–subunit complex to bind to the usher and is required to drive a conformational change in the latter that primes it for pilus biogenesis[10,21,22]. The molecular nature of this activation process is unknown. To get a direct comparison between the FimC–FimH-engaged form and the apo form of the type 1 pilus usher, we crystallized the isolated FimD translocation domain (residues 124–663) and determined its structure to 3.0 Å resolution

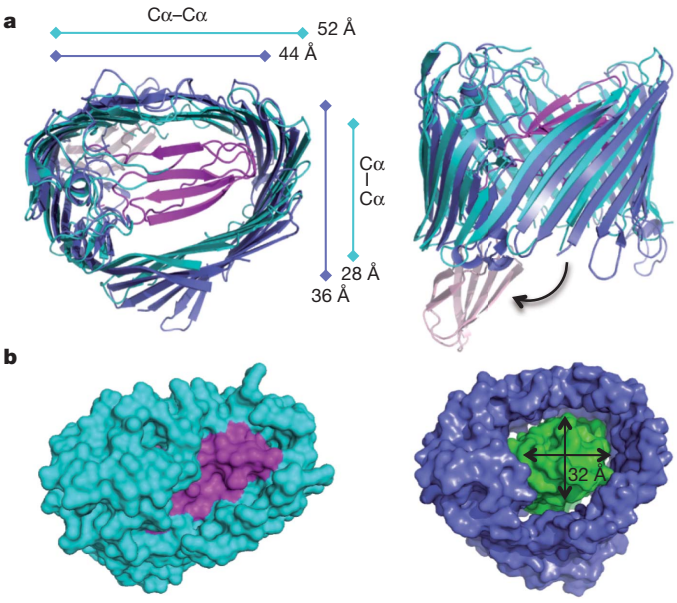

Figure 2 | Channel conformations in apo and activated (FimC–FimH-engaged) FimD usher. **a**, Top (left) and side (right) view ribbon representations of the superimposed apo-FimD (cyan) and activated FimD (slate) β-barrel. The plug domain in the channel lumen in apo FimD (magenta) rotates into the periplasm following FimD activation (pink). **b**, Top view surface representation of the apo-FimD (left) and activated FimD (right, for clarity, showing only the translocation channel and FimH lectin domain, FimH$_L$). The plug and FimH$_L$ are coloured magenta and green, respectively.

(Fig. 2 and Supplementary Fig. 5a). Apo-FimD closely resembles the structure of the PapC translocation domain (r.m.s.d. (root mean squared deviation) for corresponding Cα atoms of 1.7 Å). It is composed of a kidney-shaped 24-stranded β-barrel occluded by a plug domain (residues 241–324). The structure of the translocation domain in the FimC–FimH-engaged usher shows a marked conformational change in the β-barrel. The 24-stranded β-barrel rearranges from an oval-shaped pore with a 52 Å by 28 Å diameter to a near circular pore of 44 Å by 36 Å diameter (Cα to Cα distances; Fig. 2a, left panel). This large conformational rearrangement in the FimD translocation channel upon activation by FimC–FimH is unprecedented in β-barrel proteins, which were until now considered rigid structures.

In the apo-FimD, the translocation channel is completely sealed off by the plug domain (Fig. 2b, left panel). In the FimC–FimH -engaged complex, the plug domain is displaced into the periplasm, opening a circular channel of 32 Å now occupied by the FimH lectin domain (Fig. 2b, right panel). In apo-FimD the plug domain makes close contacts with the inner wall of the β-barrel, burying 2,738 Å^2 of surface area (Fig. 2b, left panel). In contrast, in the ternary complex, the β-barrel–FimH interface buries 1,590 Å^2 of surface area and includes fewer contacts with FimH compared to the β-barrel–plug interface in the apo form (Fig. 2b, right panel): only 6 β-barrel Cα atoms lie within 5 Å from FimH in FimD–FimC–FimH, compared to 39 β-barrel Cα atoms lying within 5 Å of the plug in apo-FimD. The more distant contact in the ternary complex structure probably provides room for the variability in subunit diameter among the different subunit types and also might facilitate translocation through the pore (Supplementary Fig. 5c, d).

Usher contains two chaperone–subunit binding sites

So far, the only region of the usher known to bind chaperone–subunit complexes is the usher N-terminal domain (NTD)[16–18]. The FimD–FimC–FimH structure now shows the existence of a second binding site on the usher, located at the C-terminal domains, CTD1 and CTD2 (Figs 1c and 3a). The FimC–FimH complex contacts the FimD usher over a surface area of 3,802 Å^2. Apart from the interaction of the FimD channel with the FimH lectin domain (see above), the most extensive interaction with the FimC–FimH complex is formed by the usher CTD1 (Fig. 3a and Supplementary Fig. 6a). CTD1 contacts the FimH lectin domain and FimC over a surface area of 621 Å^2 and 422 Å^2, respectively. Contact area between CTD2 and the FimC–FimH complex is 504 Å^2 large and is primarily with FimC. Removal of the CTDs or of CTD2 alone or point mutations in CTD1 abrogate pilus biogenesis (see ref. 23 and this work (Supplementary Table 2)). Using electron paramagnetic resonance (EPR) spectroscopy we also demonstrate that subsequent subunits localize to the CTDs binding site after undergoing DSE (Fig. 3c and Supplementary Fig. 7). Moreover, these complexes are fully functional, that is, able to incorporate the next subunit into the nascent pilus (Supplementary Figs 2b, c).

Other than its interaction with the CTDs, the FimC–FimH complex also comes into contact with the usher plug domain and the NTD (Fig. 3b and Supplementary Fig. 6b). The contact surface area between the plug and the FimH lectin domain is significant (474 Å^2). Although the NTD is located within proximity of the FimH pilin domain, the small contact surface area of 189 Å^2 and its low shape complementarity[24] of 0.45 indicate a weak interaction (Supplementary Fig. 6b). Notably, this contact zone does not overlap with the known, canonical chaperone–subunit binding site at the NTD (see later and Supplementary Fig. 6c).

When comparing the interface between FimD CTDs and FimC–FimH in the FimD–FimC–FimH structure with the interface between the FimD NTD and FimC–FimH in the structure of the NTD–FimC–FimH$_P$ complex reported previously[17], it becomes apparent that the binding sites overlap (Supplementary Fig. 8).

Thus, the usher contains two chaperone–subunit binding sites and the question arises whether these are mutually exclusive for chaperone–subunit binding or rather operate in concert, and if so, in what sequence.

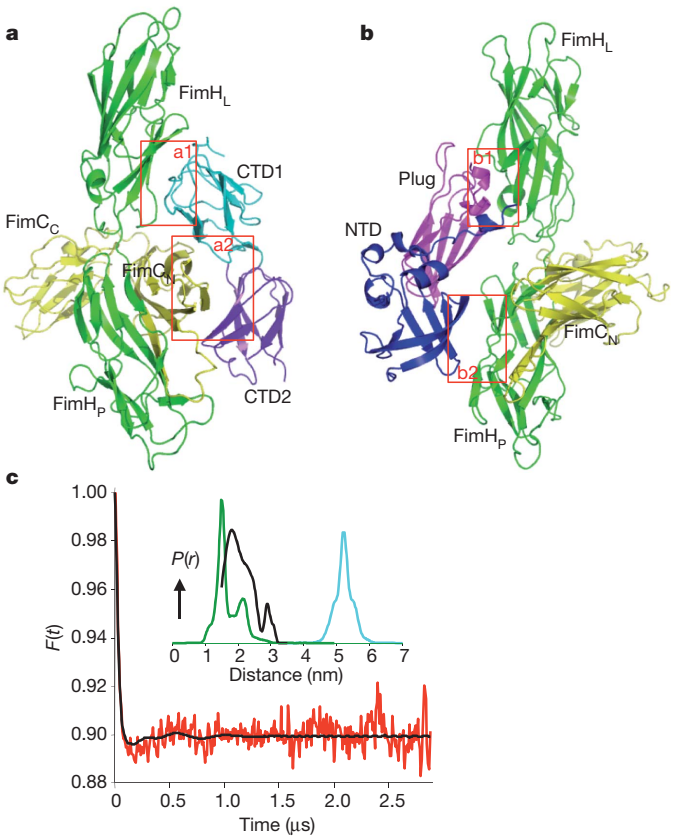

Figure 3 | FimC–FimH interactions with FimD in the FimD–FimC–FimH complex. **a**, **b**, Side view of the ribbon representation of the FimC–FimH interface with the FimD CTDs (**a**) and with the FimD plug and NTD, as found in the FimD–FimC–FimH complex (**b**). For clarity, only the respective FimD domains are shown. The boxed interfaces (a1, FimH–CTD1; a2, FimC–CTD2; b1, FimH–plug and b2, FimH–NTD) are described in the text and shown in detail in Supplementary Fig. 6. Colour coding is as in Fig. 1. **c**, DEER measurement of the distance between two nitroxide spin labels, one on residue 756 of FimD (located in CTD2) in the FimD–FimC–FimH complex, and the other on residue 74 of FimC in the FimC–FimG complex (see details and controls in Methods and Supplementary Fig. 7; see also Supplementary Fig. 7 for results of distance measurements by EPR between residue 774 of FimD CTD2 and residue 74 of FimC). The Form factor (main graph; red line), the fit to the data using DeerAnalysis2010 (main graph; black line; ref. 38), and the distance distribution derived from the data (inset; black line) are shown. For comparison, we include the distance distribution predicted by MMM[39] from the crystal structure of FimD–FimC–FimH, assuming that the position of FimC–FimG is similar to the previously bound chaperone–subunit complex FimC–FimH (green line) and the distance distribution from a model structure of FimD–FimC–FimH where FimC–FimG was positioned at the NTD as in ref. 17 (cyan line; see Supplementary Fig. 7a). It can be seen that the vast majority of the distance distribution obtained experimentally overlaps with that predicted when FimC–FimG locates at the CTDs. A minor fraction corresponding to a distance around 3 nm suggests a conformational equilibrium in solution.

A single usher protomer forms a pilus assembly machine

Chaperone/usher pili extend by step-wise addition of new chaperone–subunit complexes at the base of the growing fibre. Because the last incorporated chaperone–subunit complex is known to remain bound on the usher[18,22], the usher requires two chaperone–subunit binding sites for function. The FimD–FimC–FimH structure and the EPR data presented here demonstrate that subunits at the base of the fibre are bound to the CTDs, with the NTD lying idle. To investigate whether in the FimD–FimC–FimH complex the NTD is able to recruit the next chaperone–subunit complex, we superimposed the known structure of the FimD NTD bound to FimC–FimF[25] (the structure of the NTD–FimC–FimG complex is not available) onto the NTD in the FimD–FimC–FimH crystal structure (Fig. 4a, b). This superimposition

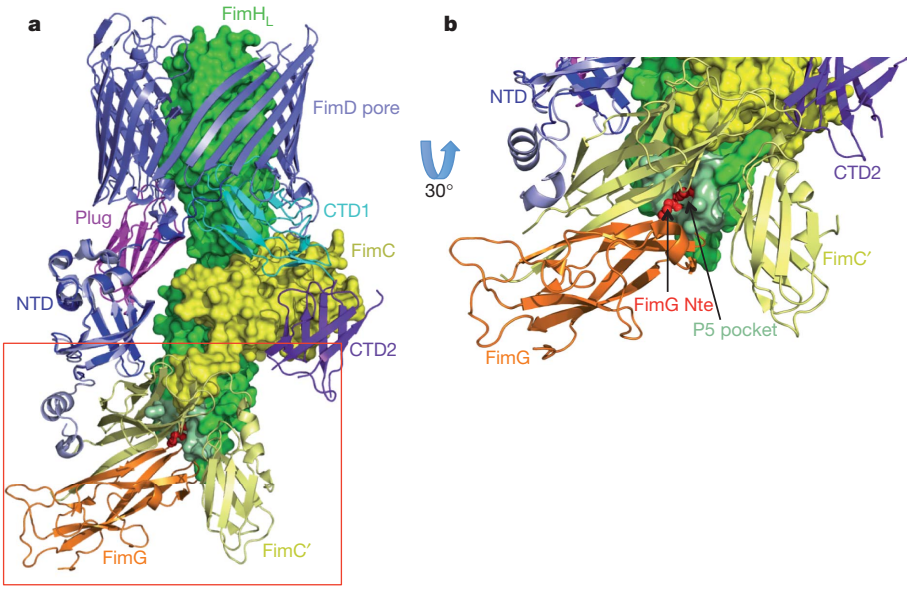

Figure 4 | Chaperone–subunit incorporation cycle at the FimD usher. **a**, Side view of the FimD–FimC–FimH complex (FimC–FimH in surface representation) with a new chaperone–subunit complex (FimC′–FimG, yellow–orange, respectively) modelled at the NTD binding site (the model is from PDB 3BWU; that is, based on the crystal structure of FimD NTD alone bound to FimC–FimF). **b**, Clipped view of the (FimC′–FimG)–(FimC–FimH) contact zone (boxed area in **a**), showing positioning of the FimG N-terminal extension (FimG Nte; in red) above the P5 pocket in the FimC–FimH complex (FimC–FimH in yellow–green, the P5 pocket shown in light green).

demonstrates that the NTD in the FimD–FimC–FimH complex is available for recruitment of a chaperone–subunit complex without steric clashes with the FimC–FimH complex bound at the CTDs. The requirement of an accessible NTD was tested by an *in vitro* DSE experiment, where the chaperone–subunit binding site of the NTD of the purified FimD–FimC–FimH complex was blocked by a bulky molecule (Supplementary Fig. 9). The inactivation of the NTD results in a near loss of further subunit incorporation, indicating that the NTD indeed acts as the recruitment site for new chaperone–subunit complexes[16–18].

The superimposition presented in Fig. 4a provides unique insights into the catalytic mechanism of a monomeric usher. The ability of the Nte of an incoming subunit to initiate the DSE reaction with the previously assembled subunit is crucially dependent on a defined binding site in that subunit, called the P5 site[26] (Supplementary Fig. 1). The P5 site allows the incoming Nte to access the hydrophobic groove of the preceding subunit, allowing it to displace the chaperone donor strand in a step-wise zip-in-zip-out mechanism[26–29]. The *in silico* model of FimC–FimF docked at the NTD of the FimD–FimC–FimH complex shows that the newly recruited subunit comes into close proximity with the FimH pilin domain, representative for the subunit that resides at the base of the growing fibre (Fig. 4a). Strikingly, the Nte of the subunit bound at the NTD lies directly above the P5 pocket of the subunit bound at the CTDs, perfectly positioned to initiate the DSE reaction (Fig. 4b). Together, the active recruitment of new chaperone–subunit complexes to the usher NTD and their ideal positioning with respect to the penultimate chaperone–subunit complex located at the CTDs provide a rationale for the catalytic ability of the usher (Supplementary Fig. 10). In the proposed model for the catalytic cycle, the chaperone–subunit complex at the base of the growing pilus fibre resides at the usher's CTDs. New subunits are recruited to the NTD and brought into ideal orientation to undergo DSE with the subunit bound at the CTDs (now the penultimate subunit; Supplementary Fig. 10, step 1). Upon DSE, the chaperone is displaced from the penultimate subunit and dissociates from the CTDs (Supplementary Fig. 10, step 2). To reset the assembly machinery for a new incorporation, the incoming chaperone–subunit complex would need to dissociate from the NTD and be transferred to the CTDs site, concomitantly pushing the penultimate subunit into the translocation channel (Supplementary Fig. 10, steps 3 and 4, respectively). How the hand-over of the chaperone–subunit complex from the usher's NTD to the CTDs occurs remains speculative.

Conclusion

The crystal structure of FimD bound to FimC–FimH provides the remarkable view of a protein transporter caught in the act of secreting its cognate substrate. Together with the FimD translocator domain structure, it elucidates not only the mechanism of gating leading to FimH insertion into the FimD barrel, but also the subsequent steps of subunit polymerization and nascent pilus translocation. Pilicide compounds recently shown to inhibit pilus biogenesis target the interface between chaperone–subunit complexes and the usher NTD[30]. The crystal structure presented here unravels a complex choreography of domain motion and protein–protein interactions that will no doubt be of crucial importance in the design of additional compounds capable of disrupting type 1 pilus biogenesis and thus inhibiting cystitis, an infectious disease that plagues millions of individuals worldwide.

METHODS SUMMARY

Purification and crystallization. FimD–FimC–FimH with a Strep-tag at the C terminus of FimD was purified as described previously with an additional Strep-tag affinity chromatography step[15]. After addition of trypsin (which removes 21 residues at the N terminus of FimD and cleaves its β13–14 loop), the complex was crystallized by hanging-drop vapour diffusion. The 6×His-tagged FimD translocation domain (residues 124–663) was purified by Ni-NTA affinity and size exclusion chromatography, and crystallized by hanging-drop vapour diffusion.
Structure determination and refinement. The crystals of the FimD–FimC–FimH complex contained two ternary complexes per asymmetric unit, related by a pseudotranslation. The chaperone–subunit (FimC–FimH) or usher domains, for which the structures (NTD) or structures of homologous domains (PapC translocation domain and plug, PapC CTD2) were available, were located individually using molecular replacement, as implemented in Phaser[31] and Molrep[32]. CTD1 was built manually using Coot[33]. Refinement with Refmac[34,35] converged to a model with an R factor of 0.219 and an R_{free} of 0.277. The structure of the FimD translocation domain was solved by molecular replacement with the equivalent PapC structure (PDB code 2VQI) as a search model using Phaser[31]. The structure was built in Coot[33], and refined in Phenix[36] to an R factor of 0.229 and R_{free} of 0.305.
DSE assay. The FimD–FimC–FimH complex was mixed with fluorescently labelled FimC–FimG, where FimG was labelled with Alexa 647 on FimG residue 92. DSE progression was monitored by the appearance of the fluorescent FimG–FimH band

on SDS–PAGE gels. For DSE experiments involving a FimD–FimC–FimH complex with a bulky molecule blocking NTD binding, FimD was reacted with Alexa 594 on residue 109.

EPR spectroscopy. The FimD–FimC–FimH complex was spin-labelled on residue 756 or residue 774 of FimD. The FimC–FimG complex was spin-labelled on residue 74 of FimC. Double electron–electron resonance (DEER) measurements for distance determination were performed as described previously[37].

Full Methods and any associated references are available in the online version of the paper at www.nature.com/nature.

Received 1 September 2010; accepted 13 April 2011.

1. Mulvey, M. A. *et al.* Induction and evasion of host defenses by type 1-piliated uropathogenic *Escherichia coli*. *Science* **282,** 1494–1497 (1998).
2. Sauer, F. G., Remaut, H., Hultgren, S. J. & Waksman, G. Fiber assembly by the chaperone-usher pathway. *Biochim. Biophys. Acta* **1694,** 259–267 (2004).
3. Waksman, G. & Hultgren, S. J. Structural biology of the chaperone-usher pathway of pilus biogenesis. *Nature Rev. Microbiol.* **7,** 765–774 (2009).
4. Jones, C. H. *et al.* FimH adhesin of type 1 pili is assembled into a fibrillar tip structure in the Enterobacteriaceae. *Proc. Natl Acad. Sci. USA* **92,** 2081–2085 (1995).
5. Hahn, E. *et al.* Exploring the 3D molecular architecture of *Escherichia coli* type 1 pili. *J. Mol. Biol.* **323,** 845–857 (2002).
6. Le Trong, I. *et al.* Structural basis for mechanical force regulation of the adhesin FimH via finger trap-like β sheet twisting. *Cell* **141,** 645–655 (2010).
7. Vetsch, M. *et al.* Pilus chaperones represent a new type of protein-folding catalyst. *Nature* **431,** 329–333 (2004).
8. Barnhart, M. M. *et al.* PapD-like chaperones provide the missing information for folding of pilin proteins. *Proc. Natl Acad. Sci. USA* **97,** 7709–7714 (2000).
9. Jacob-Dubuisson, F., Striker, R. & Hultgren, S. J. Chaperone-assisted self-assembly of pili independent of cellular energy. *J. Biol. Chem.* **269,** 12447–12455 (1994).
10. Nishiyama, M., Ishikawa, T., Rechsteiner, H. & Glockshuber, R. Reconstitution of pilus assembly reveals a bacterial outer membrane catalyst. *Science* **320,** 376–379 (2008).
11. Sauer, F. G. *et al.* Structural basis of chaperone function and pilus biogenesis. *Science* **285,** 1058–1061 (1999).
12. Choudhury, D. *et al.* X-ray structure of the FimC-FimH chaperone-adhesin complex from uropathogenic *Escherichia coli*. *Science* **285,** 1061–1066 (1999).
13. Zavialov, A. V. *et al.* Structure and biogenesis of the capsular F1 antigen from *Yersinia pestis*: preserved folding energy drives fiber formation. *Cell* **113,** 587–596 (2003).
14. Sauer, F. G., Pinkner, J. S., Waksman, G. & Hultgren, S. J. Chaperone priming of pilus subunits facilitates a topological transition that drives fiber formation. *Cell* **111,** 543–551 (2002).
15. Remaut, H. *et al.* Fiber formation across the bacterial outer membrane by the chaperone/usher pathway. *Cell* **133,** 640–652 (2008).
16. Nishiyama, M., Vetsch, M., Puorger, C., Jelesarov, I. & Glockshuber, R. Identification and characterization of the chaperone-subunit complex-binding domain from the type 1 pilus assembly platform FimD. *J. Mol. Biol.* **330,** 513–525 (2003).
17. Nishiyama, M. *et al.* Structural basis of chaperone-subunit complex recognition by the type 1 pilus assembly platform FimD. *EMBO J.* **24,** 2075–2086 (2005).
18. Ng, T. W., Akman, L., Osisami, M. & Thanassi, D. G. The usher N terminus is the initial targeting site for chaperone-subunit complexes and participates in subsequent pilus biogenesis events. *J. Bacteriol.* **186,** 5321–5331 (2004).
19. Shu Kin So, S. & Thanassi, D. G. Analysis of the requirements for pilus biogenesis at the outer membrane usher and the function of the usher C-terminus. *Mol. Microbiol.* **60,** 364–375 (2006).
20. Ford, B. *et al.* Structural homology between the C-terminal domain of the PapC usher and its plug. *J. Bacteriol.* **192,** 1824–1831 (2010).
21. Munera, D., Hultgren, S. & Fernandez, L. A. Recognition of the N-terminal lectin domain of FimH adhesin by the usher FimD is required for type 1 pilus biogenesis. *Mol. Microbiol.* **64,** 333–346 (2007).
22. Saulino, E. T., Thanassi, D. G., Pinkner, J. S. & Hultgren, S. J. Ramifications of kinetic partitioning on usher-mediated pilus biogenesis. *EMBO J.* **17,** 2177–2185 (1998).
23. Li, Q. *et al.* The differential affinity of the usher for chaperone-subunit complexes is required for assembly of complete pili. *Mol. Microbiol.* **76,** 159–172 (2010).
24. Lawrence, M. C. & Colman, P. M. Shape complementarity at protein/protein interfaces. *J. Mol. Biol.* **234,** 946–950 (1993).
25. Eidam, O., Dworkowski, F. S., Glockshuber, R., Grutter, M. G. & Capitani, G. Crystal structure of the ternary FimC–$FimF_t$–$FimD_N$ complex indicates conserved pilus chaperone–subunit complex recognition by the usher FimD. *FEBS Lett.* **582,** 651–655 (2008).
26. Remaut, H. *et al.* Donor-strand exchange in chaperone-assisted pilus assembly proceeds through a concerted β strand displacement mechanism. *Mol. Cell* **22,** 831–842 (2006).
27. Verger, D., Miller, E., Remaut, H., Waksman, G. & Hultgren, S. Molecular mechanism of P pilus termination in uropathogenic *Escherichia coli*. *EMBO Rep.* **7,** 1228–1232 (2006).
28. Rose, R. J. *et al.* Unraveling the molecular basis of subunit specificity in P pilus assembly by mass spectrometry. *Proc. Natl Acad. Sci. USA* **105,** 12873–12878 (2008).
29. Verger, D. *et al.* Structural determinants of polymerization reactivity of the P pilus adaptor subunit PapF. *Structure* **16,** 1724–1731 (2008).
30. Pinkner, J. S. *et al.* Rationally designed small compounds inhibit pilus biogenesis in uropathogenic bacteria. *Proc. Natl Acad. Sci. USA* **103,** 17897–17902 (2006).
31. McCoy, A. J. Solving structures of protein complexes by molecular replacement with *Phaser*. *Acta Crystallogr. D* **63,** 32–41 (2007).
32. Vagin, A. & Teplyakov, A. Molecular replacement with *MOLREP*. *Acta Crystallogr. D* **66,** 22–25 (2010).
33. Emsley, P. & Cowtan, K. *Coot*: model-building tools for molecular graphics. *Acta Crystallogr. D* **60,** 2126–2132 (2004).
34. Murshudov, G. N. *et al. REFMAC*5 for the refinement of macromolecular crystal structures. *Acta Crystallogr. D* **67,** 355–367 (2011).
35. Collaborative Computational Project, number 4. The *CCP*4 suite: programs for protein crystallography. *Acta Crystallogr. D* **50,** 760–763 (1994).
36. Adams, P. D. *et al. PHENIX*: a comprehensive Python-based system for macromolecular structure solution. *Acta Crystallogr. D* **66,** 213–221 (2010).
37. Pannier, M., Veit, S., Godt, A., Jeschke, G. & Spiess, H. W. Dead-time free measurement of dipole-dipole interactions between electron spins. *J. Magn. Reson.* **142,** 331–340 (2000).
38. Jeschke, G. *et al.* DeerAnalysis2006—a comprehensive software package for analyzing pulsed ELDOR data. *Appl. Magn. Reson.* **30,** 473–498 (2006).
39. Polyhach, Y., Bordignon, E. & Jeschke, G. Rotamer libraries of spin labelled cysteines for protein studies. *Phys. Chem. Chem. Phys.* **13,** 2356–2366 (2011).

Supplementary Information is linked to the online version of the paper at www.nature.com/nature.

Acknowledgments This work was funded by Medical Research Council grant 85602 to G.W., NIH grant GM62987 to D.G.T., NIH grants 49950, 29549 and 48689 to S.J.H., and NIH grant GM74985 and BNL LDRD grant 10-16 to H.L.; H.R. is supported by a VIB Young PI project grant and the Odysseus program of the FWO-Vlaanderen. K.F.P. is supported by a Schrödinger Fellowship from the Austrian Science Fund, project J 2959-N17. We thank the staff of beamlines X25 and X29 at NSLS, the staff of beamline ID23-1 at ESRF, N. Cronin for technical assistance during data collection, and H. Saibil and E. Orlova for comments on the manuscript.

Author contribution G.P. produced the FimD–FimC–FimH complex, grew the crystals of this complex, collected X-ray crystallographic data, and initiated the determination of the structure by molecular replacement, and participated in the building and refinement of the structure. H.R. produced the FimD–FimC–FimH complex, trained G.P., supervised the work, analysed the structures and wrote the paper. T.W. grew crystals of the FimD translocation domain, collected X-ray crystallographic data, and determined the structure. W.J.A. set up the DSE assay and prepared the samples for EPR. K.F.P. carried out the EPR experiments, which were analysed by K.F.P., M.B.A.K. and C.W.M.K.; A.L. completed the structure determination of the FimD–FimC–FimH complex, built and refined the structure. N.S.H., E.V., J.S.P. and B.F. cloned and purified the translocation domain of FimD, and cloned and analysed the FimD CTD mutants. S.G. participated in the building and refinement of the FimD–FimC–FimH structure and analysed the structure. J.Y. carried out the native mass spectrometry experiments on the FimD–FimC–FimH complex. C.W.M.K supervised the EPR work. H.L., S.J.H. and D.G.T. supervised the work on apo-FimD, analysed the structures, and wrote the paper. G.W. supervised the work on FimD–FimC–FimH, analysed the structures, and wrote the paper.

Author Information Structure factors and coordinates have been deposited in the Protein Data Bank (entry codes 3RFZ and 3OHN for coordinates and structure factors of the FimD–FimC–FimH complex and the translocation domain of FimD, respectively). Reprints and permissions information is available at www.nature.com/reprints. The authors declare no competing financial interests. Readers are welcome to comment on the online version of this article at www.nature.com/nature. Correspondence and requests for materials should be addressed to G.W. (g.waksman@ucl.ac.uk or g.waksman@bbk.ac.uk) or D.G.T. (david.thanassi@stonybrook.edu).

METHODS

Expression and purification of the outer membrane FimD–FimC–FimH complex. *Escherichia coli* strain B834 (Novagen) was transformed with two plasmids: pETS1001 encoding *fimC*$_{His}$*H* under arabinose control and pAN2 encoding *fimD* under IPTG control[22]. A *strep*-tag II (SA-WSHPQFEK) was added to the C terminus of FimD by the SLIM protocol (site-directed ligase independent mutagenesis[40]; Supplementary Table 3). Bacteria were grown in TB media containing kanamycin and spectinomycin at 37 °C. At $D_{600} = 1.0$, the culture was induced with 100 μM isopropyl-β-D-thiogalactoside (IPTG) and 0.1% (w/v) L-arabinose with a supplement of 0.1% (v/v) glycerol. The induced bacteria were grown for 48 h at 16 °C.

Outer membranes were prepared as described in ref. 15. Outer membrane proteins were solubilized in 20 mM Tris-HCl, pH 8.5, 120 mM NaCl, 1.5% (w/v) dodecylmaltopyranoside (DDM; Anatrace) and protease inhibitors cocktail (Calbiochem) for 30 min at room temperature. The extract was cleared by ultracentrifugation (45 min at 100,000*g*, 4 °C), loaded onto a streptavidin column, washed with 100 mM Tris-HCl, pH 8.5, 120 mM NaCl, 0.05% (w/v) DDM), and the bound fraction eluted with the same buffer containing 2.5 mM D-desthiobiotin.

Limited proteolysis of the purified FimD–FimC–FimH complex was carried out by adding directly trypsin (Sigma) to the *strep*-tag II affinity eluted fraction, with a ratio of 1:50 (w/w) of enzyme to substrate for 3 h at room temperature. Trypsin removes 21 amino acids at the N terminus of the FimD usher (cut after R21) and cleaves the usher translocation domain at loop β13–14 after residue K469, as assessed by N-terminal sequencing. Overall, the trypsin-digested complex has a molecular mass of 141 kDa compared to 144 kDa for the undigested complex (both molecular masses were assessed by mass spectrometry). Such a very minor trimming of the complex was crucial to obtain crystals, presumably removing sequences preventing crystal packing. The digested FimD–FimC–FimH was loaded onto a nickel affinity column, washed with 20 mM Tris-HCl, pH 8.5, 120 mM NaCl, 0.05% (w/v) DDM and 25 mM imidazole, detergent-exchanged with 20 mM Tris-HCl, pH 8.5, 120 mM NaCl, 2 mM LDAO (Anatrace) and 25 mM imidazole, and eluted with that same buffer containing 250 mM imidazole. 0.8% (v/v) of tetraethylene glycol monooctyl ether (C8E4; Anatrace) was then added to the nickel-affinity-eluted fraction before concentration using a 100 kDa cut-off spin concentrator (Amicon) and loading onto a HiLoad Sephacryl S300 16/60 (GE Healthcare) gel filtration column in 20 mM Tris-HCl, pH 8.5, 50 mM NaCl, 2 mM LDAO and 0.8% (v/v) C8E4. The digested FimD–FimC–FimH complex eluted as a single peak and was concentrated using a 100 kDa cut-off spin concentrator (Amicon).

Expression and purification of the FimD translocation domain. The FimD translocation domain (residues 124–663) was identified by mass spectroscopy of the limited trypsin treatment product of purified full-length FimD, and constructed using the SLIM method[40] from parental plasmid pETS4 (ref. 22), which encodes *fimD*-6×His under IPTG control (Supplementary Table 3). The final plasmid, pNH297, encodes the native FimD signal sequence followed by the translocation domain followed by a short linker sequence (GGPVAT), thrombin cleavage site (LVPRGS) and 6×His-tag.

After induction, outer membranes were obtained as described in ref. 15. Proteins were extracted from the outer membranes with 1.5% (w/v) DDM (Anatrace) in a buffer containing 25 mM Tris, pH 8.2, 300 mM NaCl, 10% (v/v) glycerol, and 1× protease inhibitors cocktail (Roche) at 4 °C overnight. The mixture was ultracentrifuged (100,000*g*, 60 min, 4 °C) to remove debris. Supernatant was loaded onto a 5-ml Ni-NTA cartridge (Qiagen) pre-equilibrated in 25 mM Tris, pH 8.2, 300 mM NaCl, 0.05% (w/v) DDM, and 20 mM imidazole. Detergent exchange was performed at this step by washing the column with 25 mM Tris, pH 8.2, 300 mM NaCl, 0.8% (w/v) C8E4 (Anatrace). The target protein was eluted in the same buffer containing a step gradient of imidazole (20 mM, 50 mM, and 300 mM). After further purification by size exclusion chromatography (Superdex-200, GE Healthcare), the FimD translocation domain was concentrated to 10–15 mg ml^{-1} in 5 mM Tris, pH 8.2, 50 mM NaCl, 1.5% (w/v) C8E4 (Anatrace).

Crystallization and data collection of the FimD–FimC–FimH complex. Trypsin-digested FimD–FimC–FimH complex crystals were grown using the vapour diffusion method at 20 °C. The crystallization drops contained 6–9 mg ml^{-1} of purified complex ($D_{280} = 8$–13), 50 mM ammonium acetate, pH 6.0–8.5, 4% (v/v) isopropanol and 770–840 mM ammonium sulphate. After 18 days, needle or blade-like crystals were flash-cooled in liquid nitrogen using the mother liquor with 30% (v/v) glycerol as cryoprotectant.

The data were collected at ESRF beamline ID23-1 (Grenoble, France) and were processed to 2.8 Å resolution using MOSFLM[41]. The integrated data were merged using POINTLESS and SCALA[42]. Space group, cell dimensions, and data collection statistics are reported in Supplementary Table 1. There was a strong non-origin peak in the Patterson map with the height of 0.37 relative to the height of the origin peak. This peak corresponded to the pseudo-translation $1/2\mathbf{c} \pm \delta\mathbf{b}$ with $\delta \approx 2.5$ Å.

Crystallization and data collection of the FimD translocation domain. The FimD translocation domain was crystallized by hanging-drop vapour diffusion method at 21 °C. Protein solution were mixed by 1:1 ratio with well solution. Plate-like crystals appeared under condition of 100 mM Na citrate, pH 4.8–6.5, 7% (w/v) PEG 4000, 100 mM NaCl, 50 mM $MgCl_2$, 20 mM spermine HCl. Crystals were flash-cooled in liquid nitrogen using mother liquor containing 30% (v/v) MPD as cryoprotectant.

Data were collected at beamline X25 at the National Synchrotron Light Source and processed to 3.0 Å resolution with HKL2000 (ref. 43). Space group, cell dimensions and data collection statistics are reported in Supplementary Table 1.

Structure determination and refinement of the FimD–FimC–FimH complex. The structure contains nine types of different domains in three different polypeptide chains (FimC and FimH contain two domains each and FimD contains five domains). Structural information was available for all individual domains but one, CTD1. The method used for location of the first three structural units (FimC, FimH, and the translocation domain of FimD) was the standard molecular replacement search (equivalent to the search in the Patterson map) implemented in both Phaser[31] and Molrep[32]. The three methods used for location of the plug, NTD and CTD2 were variants of the search in the electron density map implemented in Molrep. All three methods use $2F_o - F_c$ type maps from a refined partial structure, map coefficients from Refmac[34] being used in this work. (1) The first method uses conventional rotation function (RF) against structure amplitudes from the map masked by the partial structure to find orientation of the model, and the phased translation function (PTF) to find its position. (2) The second method uses spherically averaged phased translation function (SAPTF[44]) to generate a list of possible positions of the centre of mass of the model, phased rotation function (PRF) to assign an orientation to each potential position and PTF to verify and correct the position of the model. (3) The third method differs from the second one in that the PRF is replaced by the standard rotation function against structure amplitudes from the electron density in a sphere around the tested position of the centre of mass. In addition, for each of the three methods, the positions of two pseudotranslation-related copies of a model were being searched for simultaneously or one after another, and cross-checked using the clear translational peak in the native Patterson. There were no homologues with known structure for CTD1 of FimD and this domain was built manually using Coot[33] when all other structural units were located.

To locate the FimC–FimH complex, PDB codes 1KLF and 3BWU were used. Two copies were found using the standard molecular replacement. The next unit to be located was the translocation/barrel domain of FimD. The equivalent PapC domain (PDB code 2VQI) was positioned with both Phaser and Molrep using the previously found FimC–FimH substructure as a fixed model.

The resulting model did not refine well, probably because of conformational differences between bound and unbound structures. Fortunately, the latest version of Refmac[34] offered a "jelly body" refinement, which in contrast to conventional refinement favoured locally correlated changes in the atomic parameters. The "jelly body" refinement was applied to the partial structure containing FimC, FimH and the translocation domain of FimD and substantially changed the shape of the barrel, C-α atoms being shifted up to 3.8 Å.

The plug domain search model was from PDB entry code 2VQI. The six modes of Molrep described above were tried. The solution found with methods (2) and (3) placed the boundary residues of the plug in close proximity to the translocation domain residues to which the plug domain must be connected. Refinement resulted in a sensible electron density map leaving little doubts that the solution was correct.

One copy of the NTD of FimD (the search model derived from PDB entry code 1EZ3) was found by both Phaser and Molrep in all six Molrep's modes tried. The second copy was found with five out of six Molrep modes. In contrast, the CTD2 of FimD (the search model from 3I48, sequence identity 32%), which had poorer electron density than all other domains even in the final structure, was only located using method (2) including SAPTF, PRF and PTF. Moreover, one of the two CTD2 domains is less ordered than the other and the location of this domain required simultaneous search for two pseudotranslation-related copies.

Model building of the FimD–FimC–FimH complex was carried out manually in Coot[33]. Restrained refinement where no σ cutoff was applied was performed in Refmac 5.6 (ref. 34), including different NCS group restraints for each protein domains related by the pseudo-translation. The following regions had poor density and thus are not part of the final FimD model: F22–G25, S188–K195 (loop β3–4), G454–Y473 (loop β13–14) and E805–N807. A small loop in the final FimC model is also missing: S179–G182. At the end, 95% of the FimD–FimC–FimH model was built. Refinement statistics of the final model are reported in Supplementary Table 1.

Structure determination and refinement of the FimD translocation domain. Molecular replacement was carried out using the Phaser-Phenix[36] program and the PapC monomer (PDB entry code 2VQI) as search model. The FimD usher translocation domain was manually rebuilt in Coot[33] and refined (no σ cutoff applied) in Phenix. An N-terminal fragment (124–138), a middle loop (454–471), a C-terminal fragment (657–663), and the linker plus the 6×His tag were disordered and could not be traced in the model. The refinement statistics are listed in Supplementary Table 1.

DSE assay. A single cysteine mutation was introduced at position 92 of FimG (termed hereafter FimG^{S92C}) using the Quikchange site-directed mutagenesis protocol (Stratagene; Supplementary Table 3). The FimC–FimG^{S92C} complex was expressed and purified as described previously for wild-type FimC–FimG[22] then labelled with Alexa 647–C_2-maleimide (Invitrogen). The labelling reaction was carried out by incubating 100 μM protein and 160 μM fluorophore together overnight at 4 °C in a buffer consisting of 50 mM Tris-HCl pH 8.0, 150 mM NaCl and 1 mM EDTA. Excess dye was removed by gel filtration (Superdex-75 column from GE Healthcare) in labelling buffer, yielding pure FimC–FimG$^{S92C[A647]}$ as assessed by SDS–PAGE. Final protein concentration was determined using an extinction coefficient at 280 nm of 35,066 $M^{-1}\,cm^{-1}$, after correcting for the absorbance of Alexa 647 at 280 nm. Typical labelling efficiencies were between 80 and 100%.

Full-length FimD–FimC–FimH complex for donor strand exchange was purified as described above, with the following exceptions: (1) no detergent exchange was carried out on the nickel affinity column, instead the protein was eluted in a buffer consisting of 50 mM Tris-HCl pH 8.0, 150 mM NaCl, 0.05% DDM and 500 mM imidazole; and (2) the final gel filtration step was performed in a buffer consisting of 50 mM Tris-HCl pH 8.0, 150 mM NaCl, 0.05% DDM and 1 mM EDTA. The final concentration of FimD–FimC–FimH was determined using an extinction coefficient at 280 nm of 194,780 $M^{-1}\,cm^{-1}$ (based on a 1:1:1 stoichiometry within the complex, an assumption confirmed by analytical ultracentrifugation (results not shown)).

To initiate donor strand exchange, 160 nM purified FimD–FimC–FimH was mixed rapidly with 1 μM of FimC–FimG$^{S92C[A647]}$ at 4 °C, in a buffer consisting of 20 mM Tris-HCl pH 8.0, 150 mM NaCl, 1 mM EDTA and 0.05% DDM. Aliquots of reaction mix were quenched at various time intervals by mixing 10:1 with 2 M HCl. After adding SDS–PAGE loading buffer (but not boiling as boiling disrupts subunit–subunit interaction), the FimG$^{S92C[A647]}$–FimH product (identified by mass spectrometry) was separated from the FimG$^{S92C[A647]}$ substrate by SDS–PAGE. Note that FimC–FimH alone, in the absence of usher, does not react with FimC–FimG$^{S92C[A647]}$ within the time frame of the experiment. The fluorescent gel bands were visualized using an FLA-3000 fluorescence plate reader (Fujifilm), with excitation at 633 nm and a long-pass emission cutoff of 675 nm. Bands corresponding to FimG$^{S92C[A647]}$ (FimG) and FimG$^{S92C[A647]}$–FimH (FimG–FimH) were selected and quantified using Image Gauge (Fujifilm), and the background fluorescence subtracted from each band. Product formation was calculated by the equation:

$$[GH] = [G_{tot}]\frac{I_{GH}}{I_{GH}+I_G}$$

where [GH] is the concentration of FimG$^{S92C[A647]}$–FimH product formed, I_{GH} and I_G are the corrected intensities of the FimG–FimH and FimG bands respectively, and $[G_{tot}]$ is the initial concentration of FimC–FimG$^{S92C[A647]}$ used. [GH] data were converted to percentage completion by:

$$\text{Percentage completion} = 100\frac{[GH]}{[DCH]}$$

where [DCH] is the initial concentration of FimD–FimC–FimH.

Blocking the NTD of FimD. To block the chaperone–subunit binding site on the NTD, a mutation to Cys was introduced at residue 109 of FimD (Supplementary Table 3). The purified FimD^{Q109C}–FimC–FimH complex was reacted with Alexa 594 maleimide for 1 h on ice. Alexa 594 is here used as a block. DSE assay was carried out as described above using wild-type FimD–FimC–FimH, Alexa 594-labelled wild-type FimD–FimC–FimH (to control for the effect of non-specific labelling), FimD^{Q109C}–FimC–FimH and Alexa 594-labelled FimD^{Q109C}–FimC–FimH. Formation of the fluorescent FimG$^{S92C[A647]}$–FimH band was monitored as above.

EPR spectroscopy. EPR distance measurements were carried out to determine the position of the FimC–FimG chaperone–subunit complex relative to the usher CTD2 in solution. This was achieved by site-directed spin labelling of the FimD–FimC–FimH and FimC–FimG complexes with a nitroxide spin label (1-oxyl-2,2,5,5-tetramethylpyrroline-3-methyl methanethiosulphonate (MTSSL)). Cysteine residues were introduced at position 74 of FimC in the FimC–FimG complex, and separately at positions 756 and 774 of FimD in the FimD–FimC–FimH complex by QuikChange site-directed mutagenesis (Stratagene; Supplementary Table 3). FimC^{Q74C}–FimG was expressed and purified as described for the DSE assay, then labelled with MTSSL, using 20 μM protein, 400 μM MTSSL and the same buffer conditions as for fluorescent labelling (see above). FimD^{T756C}–FimC–FimH and FimD^{S774C}–FimC–FimH mutants did not have a strep-tag present; they were therefore expressed and purified as for the DSE assay but with the strep-tag affinity column omitted. Labelling was carried out before the final gel filtration step, using the same protocol as for FimC^{Q74C}–FimG but with the addition of 0.05% DDM to the labelling buffer. All mutants were exchanged into D_2O buffer to enhance the transverse relaxation time of the electron spins, which enables measurement of longer distances. The concentration of spin label was determined and corresponded to a labelling efficiency in the range 70–100%. The estimated error for the spin label efficiency is approximately ± 15% due to errors in the determination of the protein concentration and the determination of the double integral of the EPR spectra.

Solutions of 70 μM FimD$^{T756C[MTSSL]}$–FimC$^{Q74C[MTSSL]}$–FimG–FimH and 100 μM FimD$^{S774C[MTSSL]}$–FimC$^{Q74C[MTSSL]}$–FimG–FimH (50 μl) were prepared by mixing FimD$^{T756C[MTSSL]}$–FimC–FimH or FimD$^{S774C[MTSSL]}$–FimC–FimH with FimC$^{Q74C[MTSSL]}$–FimG in a ratio of 1:1. Glycerol (5%) was added as cryoprotectant. The mixture was transferred into a quartz capillary of 2 mm (inner diameter) and frozen in liquid nitrogen. Controls included mixing FimD$^{T756C[MTSSL]}$–FimC–FimH or FimD$^{S774C[MTSSL]}$–FimC–FimH with unlabelled FimC^{Q74C}–FimG or mixing unlabelled FimD^{T756C}–FimC–FimH or FimD^{S774C}–FimC–FimH with labelled FimC$^{Q74C[MTSSL]}$–FimG in a ratio of 1:1.

Continuous-wave EPR experiments were performed at 160 K on a Bruker EMXplus spectrometer operating at 9.4 GHz equipped with a 4122SHQE resonator and an Oxford Instruments ESR900 cryostat. All measurements were carried out with 0.2 mW microwave power, 100 kHz modulation frequency, 0.1 mT modulation amplitude and 10 ms conversion time and time constant.

DEER experiments were performed at 50 K on a Bruker ELEXSYS E580 spectrometer operating at 9 GHz equipped with an ER-4118-X-MS-3W resonator. The four-pulse DEER sequence was chosen with $\pi/2(\nu_{obs}) - \tau_1 - \pi(\nu_{obs}) - t - \pi(\nu_{pump}) - (\tau_1 + \tau_2 - t') - \pi(\nu_{obs}) - \tau_2 - echo$, where the observer pulse length was 16 ns for π/2 and 32 ns for π pulses. The pump pulse length was 12 ns, the long interpulse delay was $\tau_2 = 3$ μs. All other parameters were used according to ref. 37. The DEER spectra were analysed using the programme DeerAnalysis2010 (ref. 38). The background was corrected by a homology three-dimensional fit. Simulations were checked for stability according to the DeerAnalysis2010 manual.

Functional analysis of FimD CTDs. The FimDΔCTD1+2, ΔCTD2 only, and D725R+N728R mutants were derived from plasmid pETS4 using the SLIM protocol[40] (Supplementary Table 3). The expression level of the FimD mutants in the outer membrane was similar to wild-type FimD. Ability of the mutants to assemble functional pili on the bacterial surface was determined by haemagglutination assay, carried out as described previously[19].

40. Chiu, J., Tillett, D., Dawes, I. W. & March, P. E. Site-directed, Ligase-Independent Mutagenesis (SLIM) for highly efficient mutagenesis of plasmids greater than 8kb. *J. Microbiol. Methods* **73,** 195–198 (2008).
41. Leslie, A. G. The integration of macromolecular diffraction data. *Acta Crystallogr. D* **62,** 48–57 (2006).
42. Evans, P. Scaling and assessment of data quality. *Acta Crystallogr. D* **62,** 72–82 (2006).
43. Otwinowski, Z. & Minor, W. in *Methods in Enzymology* Vol. 276 (ed. Carter, C. W. Jr) Ch. 20, 307–326 (Elsevier, 1997).
44. Vagin, A. A. & Isupov, M. N. Spherically averaged phased translation function and its application to the search for molecules and fragments in electron-density maps. *Acta Crystallogr. D* **57,** 1451–1456 (2001).